Article in International Journal of Computational Science and Engineering 14(4):370 · January 2017
DOI: 10.1504/IJCSE.2017.10005741

COMPUTATIONAL INVESTIGATION INTO THE INFLUENCE OF YAW ON THE AERODYNAMICS OF A ROTATING WHEEL IN FREE AIR

T. D. Kothalawala, A. Gatto
College of Engineering, Design & Physical Sciences
Brunel University London
Kingston Lane, Uxbridge, Middlesex, UB8 3PH, UK.
E-mail: tharaka.kothalawala@brunel.ac.uk
E-mail: alvin.gatto@brunel.ac.uk

Abstract
This paper details a computational investigation into the influence of applied yaw angle on the aerodynamics of a rotating wheel in free air. The main analysis tool employed was Unsteady Reynolds-Averaged Navier-Stokes simulations with the primary aim to investigate and characterise the complex surface and near wake flow field physics of the configuration. Overall, results showed that the flow-field surrounding the wheel was principally vortical in nature with the number and strength of developed vortical structures heavily dependent on the level of applied yaw angle. Lift, drag, and side force coefficients, as well as on-surface pressures were also found to be inter-dependent to the level of yaw angle applied.

Keywords
CFD, wheel, landing gear, rotating wheel, yaw, bluff body, aerodynamics, free air.

Biographical notes
T. D. Kothalawala received his PhD from Brunel University in 2015, where he specialised in computational wheel dynamics. His research interests are related to CFD applications in aerospace engineering.

A. Gatto received his PhD in 2001 and is the course director for Aerospace and Aviation Engineering at Brunel. He has research interests in both computational and experimental aerodynamics, flight physics, and aircraft design.

Introduction

For each of the thousands of flights taken every day all over the world, aircraft operational requirements dictate several distinct and somewhat dissimilar aircraft configurations which depend on the particular phase of flight being executed. For example, for the approach to land phase, the aircraft is typically in a high-lift, low-speed configuration with both high-lift devices and aircraft landing gear deployed and locked. Similarly, for take-off, the aircraft is configured in a high-lift, low drag configuration, with landing gear deployed prior to retraction after obtaining a positive rate of climb. During both of these critical phases of flight, all of these lift-augmentation and landing gear components are directly exposed to the outside airstream and generate highly three-dimensional, complex aerodynamic interactions, which are normally

Article in International Journal of Computational Science and Engineering 14(4):370 · January 2017
DOI: 10.1504/IJCSE.2017.10005741

characterised by large areas of flow separation and/or unsteady wake physics. These highly complex, unsteady flow-fields, are also known to generate a significant amount of noise during these phases of flight, and as such, are often a focus of both aircraft designers and their subsequent regulatory agencies who aim to reduce the exposure of this aero-acoustic noise to nearby residents[Jones(2009), Knottnerus(2009)].

For landing gear in particular, which comprise a significant proportion of total aircraft noise signatures, the problem of reducing aerodynamic noise is complicated by a lack of detailed understanding into the complex flow interactions as well as detailed knowledge of the individual contributions from the different components. These components include wheels, struts, axles, hoses, braces, and linkages, and are typically configured into a complex arrangement that remains difficult to analyse effectively [Dobrzynski (2010)]. The wheels of a landing gear, which tend to be the largest component, are a particular example of this problem as they exhibit bluff-body aerodynamics characteristics dependent on many factors such as flow separation and re-attachment positions, Reynolds number, turbulence intensity, applied yaw angle (crosswind conditions) and wheel rotation speed. Unfortunately, there exists very little consideration in the current literature on the flow physics over an isolated wheel subject to changes in these variables representing a deficiency in current understanding. If the ambitious goals of future noise reduction targets are to be met and the development of future noise reduction technologies are to be fully realised, this flow problem needs further consideration.

At the most fundamental level, the aerodynamics of an isolated landing gear wheel can be related to the flow over a low aspect ratio circular cylinder. While there can be significant differences between these two configurations such as edge profile, hub geometry, tyre tread, and rim detail, as a first step, basic insights can be gained from considering this particular flow case. For generic circular cylinders, the flow-field characteristics are known to be heavily dependent on aspect ratio, with the special case of an infinitely long circular cylinder dominated by the development of a region of stagnated flow (at the front of the cylinder), rapid acceleration as the flow moves around the cylinder surface, flow separation due to the development of increasingly severe adverse pressure gradients near the positions of maximum diameter, and finally the development of two separated free shear layers within an oscillatory wake. The seminal work of Zdravkovich (2003) details the influence of various factors on this flow case with the primary influence of decreasing aspect ratio being a corresponding decrease in drag coefficient resulting from the increasing influence on the central wake of the highly vortical, free-end aerodynamics. However, results also showed that below aspect ratios of one, which is more equivalent to the case of a landing gear wheel, a reversal of this trend exists with substantial increases in C_D found as skin friction drag begins to dominate over pressure drag contributions [Zdravkovich (2003)]. Another variable also treated in Zdravkovich (2003) and of fundamental importance to the flow over landing gear (particularly at take-off) is the application of cylinder rotation. Results from applying a rotational speed to the cylinder surface show the development of a characteristic flow asymmetry with flow separation delayed on the side of the cylinder moving in the same direction as the free stream flow and flow separation occurring earlier upstream on the side with the flow opposing the direction of rotation. Overall, this asymmetry has the fundamental effect of decreasing drag with the subsequent production of a net lift force.

Applying yaw angle to circular cylinder flow has also been investigated. Bursnall and Loftin (1951) investigated the influence of yaw angle on the aerodynamics of circular cylinders with results showing a dependence of increasing yaw angle to reductions in critical Reynolds numbers compared to the un-yawed case. This relationship was also found to become much more complicated with aspect ratio reduction down to one, with the flow-field demonstrating significantly increased asymmetric, three-dimensionality, with inherent dependencies on variables including free stream turbulence, edge profile, boundary layer condition and Reynolds number. Similar results were also found in Zdravkovich (1989) and Gerrard (1966). Smith et al (1972) also carried out investigations into the influence of applying yaw angle (up to 60°) on circular cylinder flows with results indicating an increase in C_D with increasing yaw angle. Dominant wake shedding frequency was also measured by Smith et al (1972) with the primary influence of yaw found to

produce less pronounced wake shedding magnitudes with a broader spectral base. This was thought to be caused by the increased turbulence levels evident with increasing yaw angle as the energy related to the wake shedding dissipated compared to the zero yaw case. Hayashi et al [30] followed up this work to investigate the underlying physics behind these changes showing that the shedding process is not completely uniform along the entire span of the cylinder and that the spanwise velocity component along the cylinder length has a direct influence on the shedding process.

Considering isolated wheel flows directly, there is a surprisingly little information in the current literature which details the flow physics of an isolated wheel in free-air. The related case of an isolated wheel in contact with the ground, relevant to the automotive sector, is much more prevalent [Fackrell (1974), McManus and Zhang (2006), Fackrell and Harvey (1975), Stapleford and Carr (1970), Axon (1998), Wray (2003), Dimitriou and Klansman (2006), Sprot (2013)]. Recently, an experimental investigation was undertaken into the aerodynamics of an isolated, non-rotating wheel in free-air, providing several insights into this flow case [Zhang et al (2013)]. Through the use of several experimental tools, several flow structures were identified over the wheel, including areas of flow separation and attachment around the wheel sides, within the hub detail, and over the top and bottom of the wheel as well as the generation of four distinct, asymmetrically-positioned, streamwise trailing vortices, convecting downstream from the rear face of the wheel. A near symmetric, low velocity deficit in streamwise velocity magnitude within the near rear wake of the wheel with measured surface pressure magnitudes of $C_p \approx 0$ were also identified as well as two high flow velocity regions over the top and bottom extremities of the wheel centreline with maximum mean surface pressure magnitudes of $C_p \approx -1$. Measurements of drag coefficient, in both natural and artificially tripped cases were also measured with the wheel and supporting strut combination giving a drag coefficient of C_D=0.24-0.3 for $Re_n > 0.8x10^6$. Results inferred from these measurements for the isolated-wheel itself were $C_D \approx 0.19$.

While somewhat different from the case of an isolated wheel in free-air, further useful insights can also be gained from considering the case of isolated wheels in contact with the ground. Wray (2003), Cogotti (1983), and Mears (2004) have all investigated this flow case with Wray (2003) detailing a computational study of the effect of yaw on this configuration. Using primarily the k-ε realizable turbulence model, results showed the flow-field to be dominated by the generation of pairs of vortical structures within the wake at both the top and bottom of the wheel. Cogotti (1983) and Mears (2004) conducted similar studies with results from Cogotti (1983) showing that both lift and drag peaked (and reduced thereafter) at 15° yaw. Mears (2004) investigated more moderate degrees of yaw up to 5° with results indicating a drag increase of 5% and a lift reduction of 17%.

MacCarthy (2010) also investigated the influence of moderate yaw angles on the aerodynamics of an isolated wheel in contact with the ground. From this study, one of the main influences of yaw angle on the resulting near-wake flow-field was the apparent ‘skewing’ of the entrained wake flow over the top of the wheel in the direction of yaw. The skewing of this entrained wake flow was also found to offset the positions and relative magnitudes of the generated, upper counter-rotating pair of vortices, with the bias tending to favour the windward side of the model. Interestingly, work within this study also included on the effects of exposed hub detail in non-yawed configurations showing that both an increase in overall lateral wake size, as well as drag coefficient, resulted from the use of evacuated hub detail.

As the goal of reducing aircraft noise will remain for the foreseeable future [Knottnerus(2009)], it is of great importance that the aerodynamic flow field around noisy components such as landing gear are thoroughly analysed and understood. To aid this understanding, and as a first step, these complex components can be first simplified before analysis to gain insight. This analysis methodology has been used in the past and has shown a good ability to provide useful information [Fackrell (1974), McManus & Zhang (2006)]. This is the approach adopted in the current work. Therefore, as an initial exploratory investigation, and to supplement the available literature, the current work will focus on characterising

Article in International Journal of Computational Science and Engineering 14(4):370 · January 2017
DOI: 10.1504/IJCSE.2017.10005741

the aerodynamics of an isolated wheel in free air that has both imposed yaw angle and rotational speed. This condition is a common every-day occurrence in aircraft operational flight and will represent a fundamental initial investigation prior to the consideration of more complicated multiple-component combinations.

Computational Methodology

For this study, the isolated wheel configuration selected was the A2 wheel configuration experimentally tested in Fackrell (1974). The decision to choose this configuration as the basis for the analysis was driven by the need to provide a solid foundation of experimental and computational data for subsequent validation and verification of the computational methodology and subsequent flow field dynamics. This wheel geometry also contains both hub detail approximating a simplified typical landing gear hub configuration (albeit more asymmetric normally) as well as a tyre width to diameter ratio indicative of a landing gear wheel. Moreover, the similarity of the intended study with that of the Fackrell (1974) investigation was deemed to be the most advantageous way to verify the validity of the current work, particularly with the absence of comparable, isolated-wheel, free-air investigations.

A schematic of the computational domain used is detailed in Figure 1. For all simulations, the wheel centre (width (l) and diameter (d) of 0.191m and 0.416m) was positioned at the geometric centre of the height and width of the domain, positioned at a distance z_2 downstream from the inlet plane. Positive yaw angle was applied to the wheel as defined in Figure 1. The final values selected for x_1, y_1, and z_1 as well as suitable grid density were chosen after a rigorous initial investigation involving both boundary and mesh refinement studies in which all of these variables were changed from a first initial estimate until results exhibited insensitivity with further modification. For this investigation, the scaling factors for boundary locations and grid density were applied through course and fine configurations from one-half to double the size originally selected so that an efficient mesh could be obtained [Logg (2009)]. On completion of this study, a final computational domain measuring z_1=24d in length, x_1= 4.4d in width, and y_1=6d in height, comprising 5 million structured-hexahedral cells, was selected as the baseline.

Ansys Fluent™ was the CFD solver used for this investigation. For all URANS computations, the k-ε realizable turbulence closure model was chosen. This model has been used in the past over similar bluff-body configurations with generally acceptable correlation with experimental data and convergence capabilities [McManus and Zhang (2006), Kaennakham and Moatamedi (2014)]. Moreover, the results obtained for the validation (presented in the following section) was found to be adequate, giving some confidence in the results from the URANS simulations. Other simulation methodologies such as Large Eddy Simulation (LES) [Ansys Fluent Theory Guide (2010)] or Lattice Boltzmann Method [Luo et al. (2010)] have been known to provide results with better accuracy within complex flow fields such as

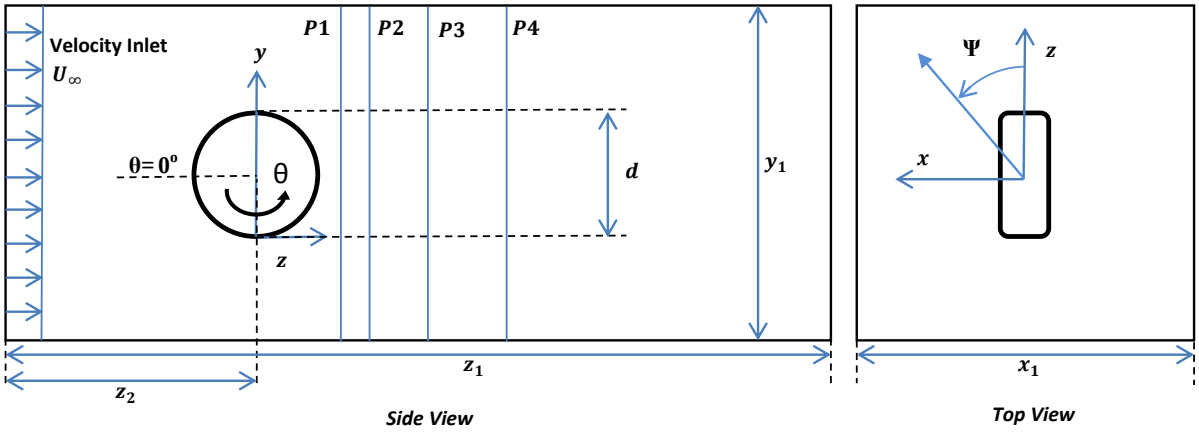

Figure 1. Computational Geometry

Article in International Journal of Computational Science and Engineering 14(4):370 · January 2017
DOI: 10.1504/IJCSE.2017.10005741

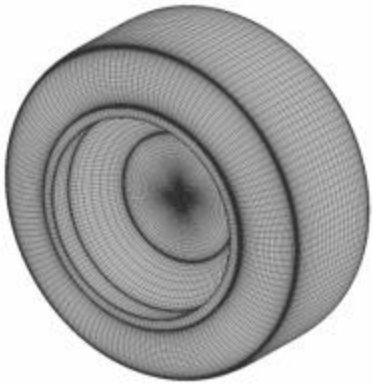

Figure 2.Wheel surface grid

this, however, the use of these methodologies are extremely computationally expensive and time consuming [Sprot (2013)]. Moreover, previous authors have used URANS modelling for similar fundamental investigations, achieving sufficient validation to experimental work and obtaining thereafter a deeper fundamental understanding of the dominant flow structures and wheel physics [McManus and Zhang (2006), Axerio-Cilies et al. (2012)].

For the current case, boundary layer modelling was implemented through the use of the enhanced wall treatment due to the complex flow structures expected and the y+ value maintained at less than 2.5 over the entire wheel. For the purpose of validating the computational methodology, the wheel was modelled as a smooth no slip wall, over a stationary isolated wheel in free air to allow comparisons to be made to the available literature. This methodology was chosen due to a lack of comparable literature for a rotating wheel configuration. To capture the effect of rotation, the wheel (Figure 2) was modelled within the computational methodology as a smooth, moving wall, with an angular velocity of 192.31rad/s (equivalent to the free stream inlet velocity U_∞=40m/s). The wheel was also set to rotate in an anticlockwise direction (θ shown in Figure 1) about the centre x-axis of the wheel. To simulate the typical crosswind approach conditions of an aircraft, yaw angles of between ψ = 0-15° in steps of 5° were selected for analysis, with the yaw angle reference centre position located at the geometric centre of the wheel (y/d=0.5). For the grids incorporating wheel yaw, the near-field region of the baseline grid (ψ = 0°) was rotated by an angle about the +y axis representative of the yaw angle required. The far-field mesh was then constructed around these yawed near-field blocks to complete the computational domain (example shown in figure 3). In total, the baseline computational domain comprised up to 80 structured blocks, positioned both within the near-field and far-field. A velocity boundary inlet condition was used for all computations with the outlet domain modelled as a pressure outlet set to standard atmospheric conditions. Turbulence intensity for both the inlet and outlet domains was set to 0.2% with all sides of the domain modelled as symmetry planes to negate the need resolve wall boundary layers. The Reynolds number, based on wheel diameter, was 1.1×10^6. All simulations were computed on a Linux based cluster as the grids required a large computing power [Lan and Deshikachar (2004)]. The results obtained from the URANS solver were obtained using a time increment of 0.00006s representing a non-dimensional time step of 0.0057 based on free stream velocity and wheel diameter. This time step was selected after initial investigations indicated that smaller time steps ($<1 \times 10^{-5}$s) had no appreciable influence on the final results obtained. For each time step, residuals were allowed to converge to a minimum standard of three orders of magnitude for 20 iterations per time step. Computational discretization was performed initially using first-order schemes for pressure, momentum and turbulence quantities to minimise computational expense before enacting second-order discretization schemes after an initial development period.

Article in International Journal of Computational Science and Engineering 14(4):370 · January 2017
DOI: 10.1504/IJCSE.2017.10005741

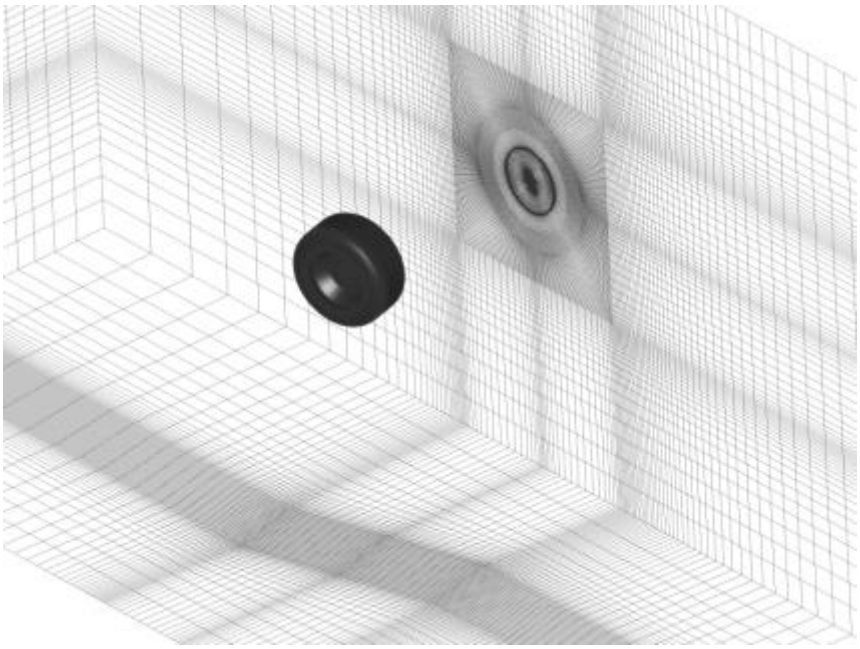

Figure 3. Computational grid with 15° yaw angle applied (flow direction from the left).

After this initial first-order development period, the flow was allowed to further develop for an additional 17 non-dimensional time units before data sampling for mean flow statistics was initiated. Mean flow quantities were thereafter calculated after a subsequent 173 non-dimensional time units.

Experimental Validation of Computational Methodology

Before presentation and discussion of the results from the computational analysis of the isolated rotating wheel in free air, where available and appropriate, both experimental and computational results available in the literature will be compared to the baseline case of the isolated, non-yawed, stationary wheel in free-air to validate and verify the computational methodology. Where possible, this validation involves the use of both mean surface data as well as near-field wake data, however, particularly for the latter, limited data exists for comparison.

To obtain results for the baseline stationary case, the methodology was identical to that outlined in the previous section albeit with a stationary, non-moving wall boundary condition for the wheel, as discussed further in Kothalawala & Gatto (2015). As an initial comparison, Figure 4a shows the mean co-efficient of surface pressures along the wheel centreline (x/d=0) obtained from the URANS study [Kothalawala & Gatto (2015)], plotted against centreline experimental data manually extracted from literature [Zhang et al (2013), Lazos (2002)]. As illustrated in Figure 4, there is excellent agreement to Zhang et al (2013) over most of the wheel centreline circumference with maximum deviations found to be typically less than $\Delta C_P \approx 0.05$. The work from Zhang et al (2013) comprised of an experimental investigation of a similar-sized isolated wheel (with asymmetric hub detail) at a similar flow velocity. Agreement with Lazos (2002), which was extracted from the front wheel of a four-wheel landing gear model, is much less correlated, but nevertheless, does show general qualitative agreement with that of the isolated wheel flow cases presented. For both comparisons, it is evident that the URANS solution tends to predict higher mean pressure coefficients within the wake region surrounding $\theta = 180°$ than those obtained experimentally. This trend has been identified in other studies comparing both URANS to higher-order computational methods as well as experimental studies [Hedges et al (2002), Bayraktar et al (2012)]. Comparing the data included from Lazos (2002), flow separation along the centreline tends to occur earlier ($\theta \approx 150°$ & 240°) with more asymmetric wake behaviour, indicating in agreement

Article in International Journal of Computational Science and Engineering 14(4):370 · January 2017
DOI: 10.1504/IJCSE.2017.10005741

with [Lazos (2002), Lazos (2002b)], that influence of the subsequent rear wheel is significant on the aerodynamics of the front wheel of a landing gear. The presence of support struts/axles in Lazos (2002) would also complicate the wake characteristics for this configuration.

Attempts by the authors to accurately model the wheel geometry used in the experimental investigation by Zhang et al (2013) using the exact same computational criteria outlined were also performed to further validate the computational methodology used in the present study. The results for centreline surface pressure distribution from this investigation are also presented in Figure 4a and show general agreement. Comparing experimental mean pressure coefficient data obtained from Zhang et al (2013) (Figure 4b) at x/d=±0.17 from the wheel centreline to the current URANS results also show a reasonably coherent correlation between the two sets of isolated wheel data. This is particularly evident in regions on the wheel where attached flow is expected ($\theta < 120°$ and ($\theta > 240°$) with agreement degrading in areas where more complicated flow physics and flow separation occurs ($120° < \theta < 240°$). Off-centreline surface pressure is known to be very sensitive to wheel profile [Fackrell (1974)] and from Figure 4, the qualitative differences evident, together with differences in hub detail, are thought to be the main factors responsible for the observed differences in the data.

Comparisons of mean drag coefficient (C_D) between the two isolated wheel studies also show reasonably good agreement. Results of drag coefficient stated in Zhang et al (2013) for both the wheel and support sting without artificial boundary layer tripping ($Re_n > 1 \times 10^6$) were reported as $C_D \approx 0.29$-0.3. The overall drag coefficient for the present URANS study, modelling only the wheel, was measured at $C_D = 0.35$ ($Re_n = 1.1 \times 10^6$). If consideration is given to the influence of the sting drag supporting the wheel from Zhang et al (2013) whose individual drag was inferred by the current authors at $C_D \approx 0.11$ (un-tripped), the overall wheel drag coefficient reduces to $C_D \approx 0.19$. It should be noted however, that in accounting for this difference, the A2 wheel profile used in the present study, has near-symmetric, wholly evacuated hub detail allowing the generation of further flow stagnation regions within the inside of the hub region. Allowing the flow to enter this region and stagnate would further increase the overall drag of the wheel with previous studies showing differences between exposed and covered hub detail representing as much as a further 27% increase in drag [Mercker and Berneburg (1992)]. Furthermore, it should also be noted that the hub detail described in the experimental study [Zhang et al (2013)] on the 'boss' side has no perceivable evacuated area, exposing the flow field to a much more streamlined wheel side producing less internal stagnated regions of flow, and conceivably, less aerodynamic drag. This reasoning is also supported from estimates of individual wheel drag coefficients extracted from 'no hub' landing gear wheels ($C_D \approx 0.15$-0.16 [Hedges et al (2002)]). Inherently, these configurations are much more streamlined inhibiting free stream flow impingement onto downstream internal hub surfaces. Additionally, the attempted computational modelling of the experimental wheel used by Zhang et al (2013) by the authors provided a drag coefficient of $C_D = 0.26$, showing general agreement to the experimental study and good agreement with the present URANS study. URANS was also found to over-predict drag coefficients when compared to experimental results investigating other similar bluff-bodies such as cylinders [Benim et al. (2008), Benim et al. (2005)]. Fackrell (1974) has also stated that the A2 wheel configuration comprised a drag contribution from the hub of $C_D = 0.08$, yielding a net drag of $C_D = 0.27$, which shows good correlation to both the experimental study by Zhang et al (2013) and the authors attempt to model their geometry computationally.

Qualitative comparisons of the general wake dynamics observed from the current study to available literature also show general agreement. Figure 5 provides baseline wake information representative of the centreline, non-dimensional, streamwise velocity at wheel mid-width. Considering Figure 5, the baseline wake characteristics are similar in general topology to that presented in the isolated wheel experimental investigation Zhang et al (2013) and the rear wheel wake characteristics of the 4-wheel

Article in International Journal of Computational Science and Engineering 14(4):370 · January 2017
DOI: 10.1504/IJCSE.2017.10005741

complete landing gear study presented by Lazos (2002). Characteristic of this wake are the contours of

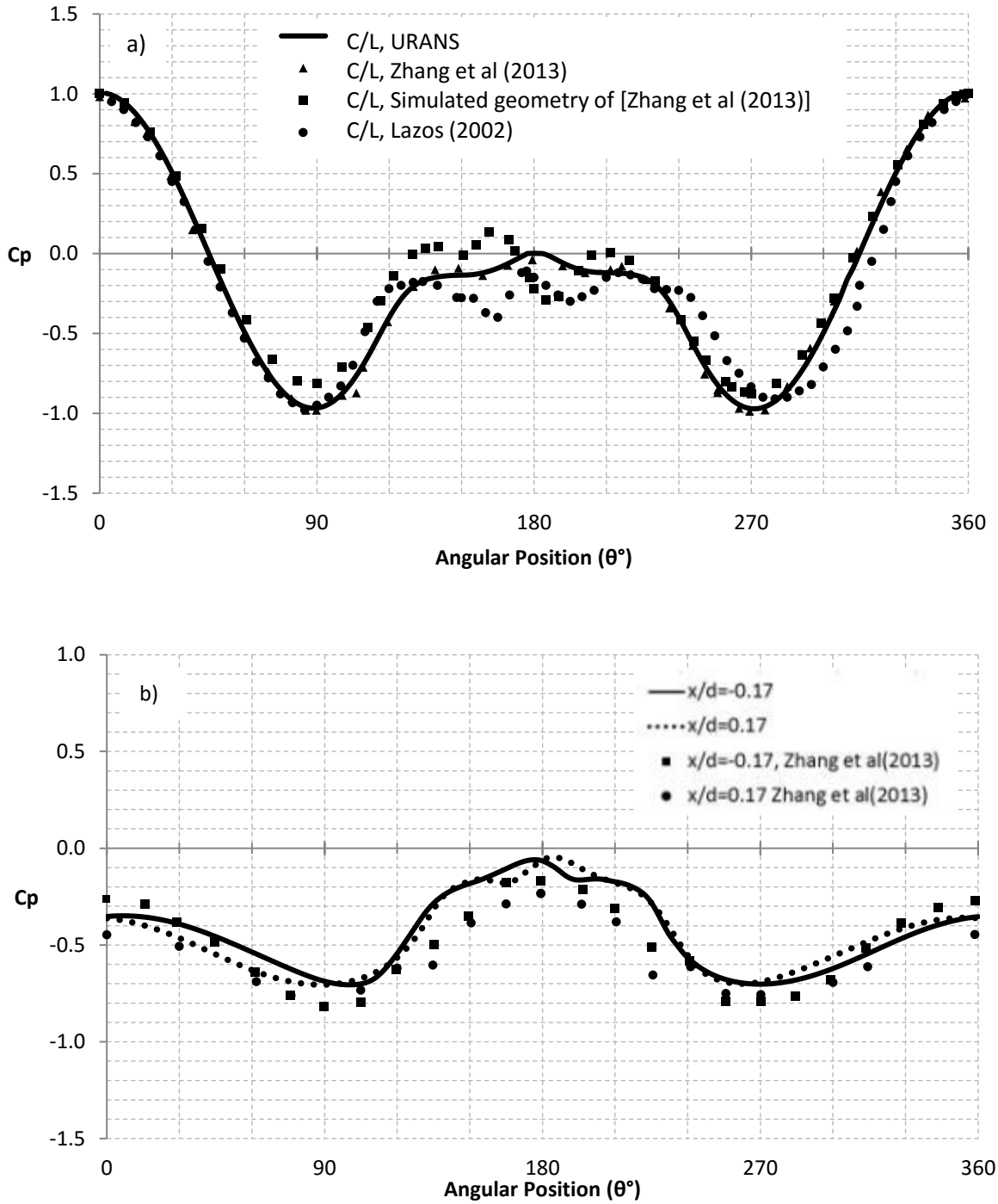

Figure 4. Comparison of mean pressure data for the stationary case conducted at Re_n =1.1 x10^6 [Kothalawala & Gatto (2015)] with experimental work at Re_n=1.3x10^6 [Zhang et al (2013)] & Re_n = 6x10^5 [Lazos (2002)]: a) centreline, b) x/d=±0.17

non-dimensional streamwise velocity magnitude emanating from directly behind the wheel with very low flow velocity experienced at wheel mid-height. URANS results from the present study, calculated within the inner-most region of the wake were very close to zero with results observed in the literature [Lazos (2002), Zhang et al (2013)] reported with a similar magnitude both behind an isolated wheel and within the wake of the rear wheel of a 4-wheel landing gear [Lazos (2002)].

Article in International Journal of Computational Science and Engineering 14(4):370 · January 2017
DOI: 10.1504/IJCSE.2017.10005741

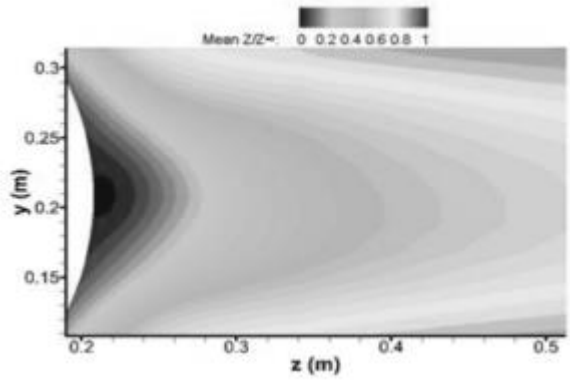

Figure 5. Contour plots of streamwise velocity at x/d=0 for Stationary results at Re_n =1.1 x10^6 [Kothalawala & Gatto (2015)].

Overall, the results used for validation, consisting of centreline & off centreline surface pressure, streamwise velocity and drag coefficient, was found to be in good agreement when compared to the literature. Moreover, the computationally modelled configuration of the experimental wheel from Zhang et al. (2013) also showed results which were in agreement when compared, therefore providing confidence in the methodology used.

Results and Discussion

Baseline flow physics

In order to compare directly the influence of applied yaw angle on the flow physics on a rotating wheel, the fundamental flow physics dominating the baseline flow case of a non-yawed, rotating wheel in free-air, is first characterised. Presented in Figures 6 and 7 are the results obtained from the URANS simulations on this flow case including non-dimensional vorticity magnitude together with mean streamwise velocity contours and streamlines, and mean velocity direction and magnitude. Figure 6 shows the cross-sectional flow-field around the rotating wheel. At the front of the wheel θ=0° (A), the flow is found to stagnate upon interacting with the surface of the wheel. Subsequent to this stagnation region, the flow is found to accelerate around both lateral sides of the wheel with a maximum mean velocity magnitude (normalised by the free-stream velocity) of 1.44. Beneath the wheel (D), where the free stream flow direction coincides with the anti-clockwise wheel rotation, a maximum mean suction pressure and normalised velocity magnitude of C_p = -1.04 and 1.37 respectively at θ = 86° occurs, before the flow is entrained by the intense up-wash directly behind the wheel. Alternatively, the normalised velocity magnitude of the flow travelling along the upper surface (Figure 6, A to B) increases up to 1.24. However, as the flow opposes the direction of wheel rotation, the flow separates earlier (B) at θ = 264° as the intense up-wash (C) along the rear surface of the wheel (induced by wheel rotation) interacts with the upper shear layer (SL_R) which propagates into the rear wake. This wake region was also found to be shifted upwards, more towards the top of the wheel, when compared to the baseline stationary wheel in free air [Kothalawala and Gatto (2015)]. The wake behind the stationary wheel is entrained within the shear layers formed after separation between θ=140° and θ=220°, whilst the wake behind the rotating wheel is entrained between the upper flow separation region at θ=264° and the lower flow detachment region at θ=145°. Figure 7 also illustrates the wake being displaced in an upward direction, as regions of vorticity are present within the upper wake region with downstream propagation into the rear wake.

Article in International Journal of Computational Science and Engineering 14(4):370 · January 2017
DOI: 10.1504/IJCSE.2017.10005741

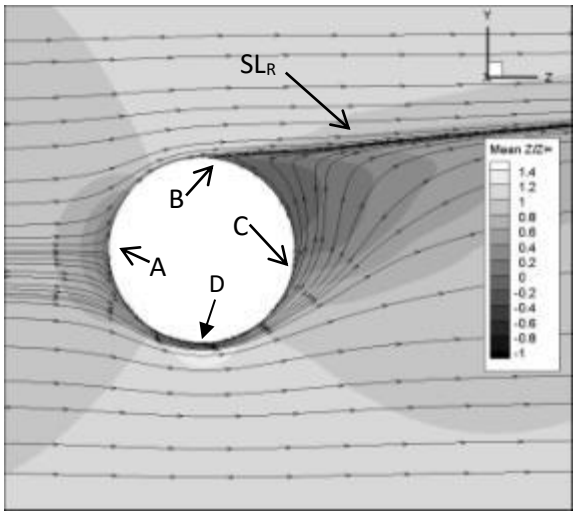

Figure 6. Cross-sectional plane on rotating wheel showing Streamlines by streamwise velocity & mean non-dimensionalised z-velocity contours at x/d=0 (Re_n =1.1 x10^6)

Within the wake, the intense up-wash (travelling directly behind the wheel at $Y/U_\infty = 0.57$) entrains the flow upwards until it interacts with the separated shear layer, forcing the flow to separate and circulate to form a pair of counter-rotating vortices (V_{1R} & V_{2R}) that propagate into the rear wake (Figure 7). This vortex formation characteristic is near symmetric about the vertical centreline of the wheel. Moreover, the intense up-wash behind this rotating wheel was found to be greater in vertical velocity (Y/U_∞) when compared to the up-wash and downwash present behind the stationary wheel which approximately provided $Y/U_\infty = \pm 0.31$ respectively. However, considering the flow-field on either side of the horizontal centreline of the wheel, the observed rear wake illustrated only two dominant vortical structures, indicating that a fundamental characteristic of the application of rotation transforms the four vortex rear wake initially observed on a stationary wheel in free air [Kothalawala and Gatto (2015)], to a two vortex wake positioned on the upper rear wake. This is also a fundamental change when compared to the number of vortical structures observed on the rear wake of a stationary wheel in contact with the ground [Fackrell J.E., (1974), McManus, J. and Zhang, X., (2006)]. The vortical structures observed in the rear wake of a stationary wheel in free air were found to be created by the flow rolling over the rear wheel edges and circulating both within the upper and lower halves of the wheel whilst being entrained by a downwash and up-wash respectively. With the flow rolling over the edges of the stationary wheel, the upper left vortex was found to circulate clockwise whilst the upper right vortex was found to circulate anticlockwise. With the application of rotation, the vortex formation characteristics have reversed as both vortices on the rotating wheel were found to be circulating in the opposing direction to that observed on the stationary wheel, when looking from behind (Figure 7). However, this was somewhat expected as the rear wake of the stationary wheel is dominated by both an up-wash travelling from beneath the wheel and a downwash travelling over the top of the wheel, forcing the flow to circulate to either side upon interacting with each other near wheel mid-height. The two vortices on the rotating wheel are formed as the intense up-wash from beneath the wheel, induced by the wheel rotation, interacts with the separated shear layer on the upper surface of the wheel forcing the flow to circulate to either side, inherently creating regions of 'horseshoe' vorticity on the upper half of the rear wake, as illustrated in Figure 7(a). This characteristic was also found to be in agreement with the counter-rotating vortex pair found on the upper rear wake of a rotating wheel in contact with the ground [Fackrell J.E., (1974), McManus, J. and Zhang, X., (2006)].

Article in International Journal of Computational Science and Engineering 14(4):370 · January 2017
DOI: 10.1504/IJCSE.2017.10005741

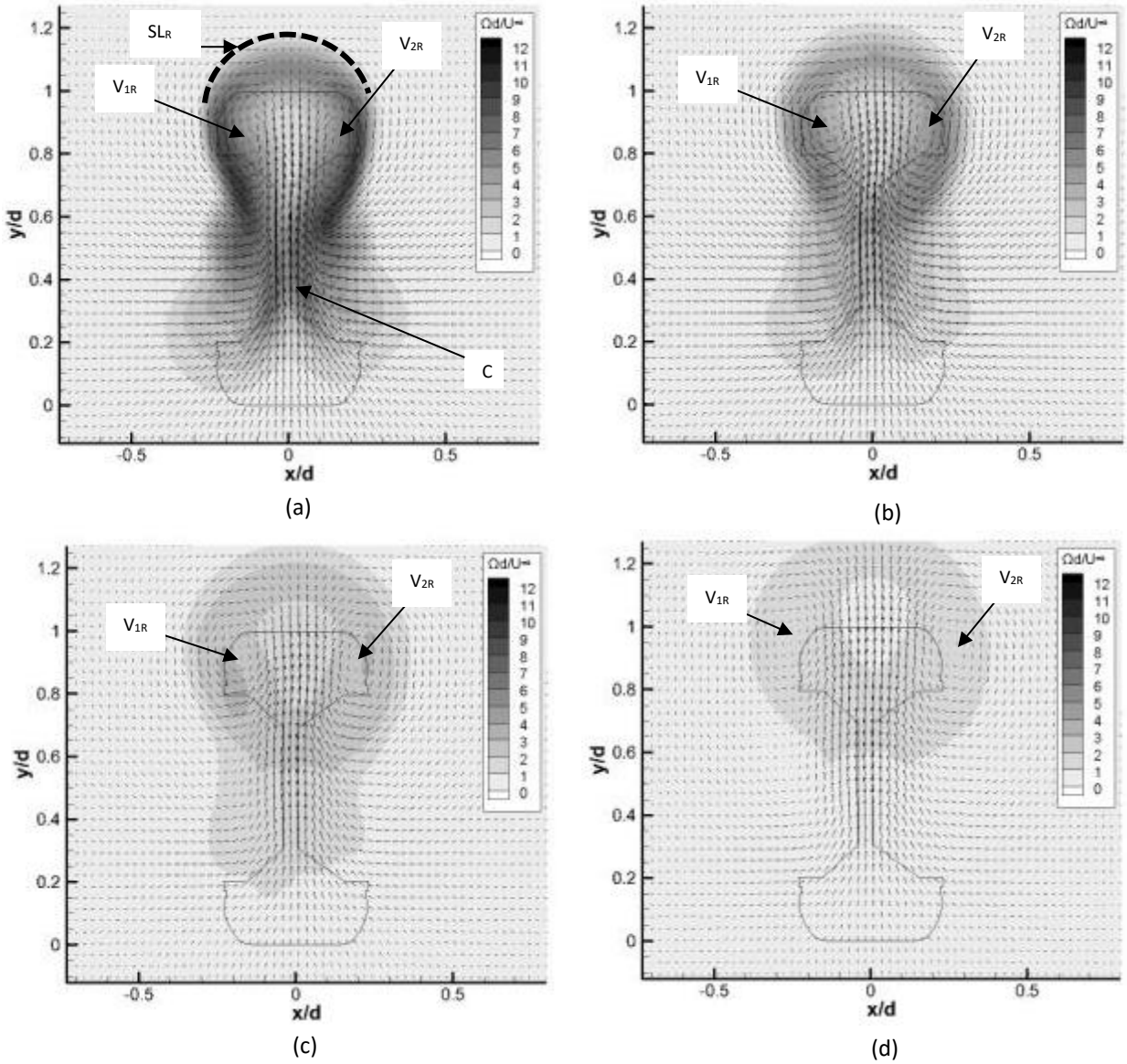

Figure 7. Non-dimensional vorticity plots for 0° yaw rotating wheel; a) z/d=0.75, b) z/d=1, c) z/d=1.5, d) z/d=2.5 (Re_n =1.1 x10^6)

To aid in understanding the wake characteristics, central vortex core magnitude and vortex core position with downstream propagation were also analysed. Considering the vorticity plot shown in Figure 7 for this rotating case in free-air, results show that at this downstream location (z/d=0.75), both position relative to the wheel centreline and vorticity magnitude intensity are near-symmetric. The initial position of the two vortices indicated V_{1R} being positioned on the -x direction, whilst V_{2R} was positioned on the +x direction, in actual fact positioned nearly symmetrically about the vertical wheel centreline. Further downstream, the vortices were found to laterally translate away from each other, as V_{1R} translates in the -x direction, whilst V_{2R} translates in the +x direction. With this translation of the two vortices in the -x & +x direction for V_{1R} & V_{2R} respectively, both vortices also continue to translate upwards in the +y direction, as illustrated in Figure 7, representing a taller wake when compared to the stationary case [Kothalawala and Gatto (2015)], and is also expected on a rotating wheel in contact with the ground [Fackrell (1974), McManus and Zhang (2006), Mears (2004)]. From flow-field interrogation, vortex core vorticity magnitudes were also found to be similar between the two vortices comprising a difference of only 12% at z/d = 0.75 as $\Omega d/U_\infty$ = 5.05 for V_{1R} and $\Omega d/U_\infty$ = 5.64 for V_{2R}.

Article in International Journal of Computational Science and Engineering 14(4):370 · January 2017
DOI: 10.1504/IJCSE.2017.10005741

With subsequent downstream propagation to z/d = 2.5 (Figure 7d), the vortex core vorticity magnitudes remained symmetric. For the case of a rotating wheel in contact with the ground [Fackrell J.E., (1974), McManus, J. and Zhang, X., (2006)], results show the generation of a 'arch-shaped' horseshoe vortex on the upper rear wake, together with a pair of counter-rotating vortices on the lower rear wake created due to flow circulation from the contact patch region. However, a significant effect of the application of rotation on a wheel in free-air is that the two lower vortices (initially observed when in contact with the ground) are not created as the flow is entrained toward the upper shear layer due to wheel rotation, only forming a two vortex wake as illustrated in Figure 7.

The Influence of Yaw Angle

Modelling the influence of yaw angle and understanding the key flow characteristics of such a flow configuration may provide some understanding of the fundamental flow characteristics representative of an aircraft landing gear wheel, either on approach or immediately after take-off, in crosswind conditions. Results presented in Kothalawala and Gatto (2015) highlighted that the principal effects of applied yaw on a stationary wheel was the initially observed four-vortex wake at zero yaw being transformed to a two-vortex wake with applied yaw angle past 5°. This two vortex wake was found to become more symmetrical about the horizontal wheel centreline with increasing yaw angle to 15°. In this present case behind a rotating wheel with zero yaw, the predominant wake structure consists of two vortices with the influence of applying yaw angle found to rotate the wake towards the windward side of the wheel. Considering the case illustrated in Figure 8, the two vortices have rotated towards the windward side of the wheel (indicated) at a yaw angle of 5° over that found from Figure 7a. The intense up-wash observed in Figure 7-C, is also skewed towards the windward side, however still remains unable to fully entrain the flow towards the windward side, as $V_{1R'}$ remains positioned towards the left hand side of the vertical centreline of the wheel.

Comparing the vorticity plot for the wheel yawed at 5° (Figure 8) to the un-yawed case (Figure 7), the two vortices have translated by $\Delta x/d = 0.08$, $\Delta y/d = -0.03$ for $V_{1R'}$ relative to V_{1R}, and $\Delta x/d = 0.01$, $\Delta y/d = -0.33$ for $V_{2R'}$ relative to V_{2R}. The two vortices that were initially positioned symmetrically about the horizontal centreline have rotated towards the windward side (clockwise when looking from behind), with the up-wash (C') from the bottom of the wheel also being skewed towards the windward side of the wheel. With further analysis comparing central vortex core vorticity magnitude and the visual size between the two vortices ($V_{1R'}$ and $V_{2R'}$), the lower vortex ($V_{2R'}$) is smaller in size but stronger than the upper vortex ($V_{1R'}$) , as $\Omega d/U_\infty = 4.32$ for $V_{1R'}$, and $\Omega d/U_\infty = 6.61$ for $V_{2R'}$ respectively at z/d = 0.75. Considering vortex core position with downstream propagation from z/d = 0.75 to z/d = 2.5 for this 5° case, $V_{1R'}$ has a 26% greater vertical displacement upwards than $V_{2R'}$, (V_{1R}': $\Delta y/d = 0.147$, $V_{2R'}$: $\Delta y/d = 0.117$). However, $V_{2R'}$ propagates downstream with a greater transverse displacement of $\Delta x/d = 0.156$ compared to $V_{1R'}$: $\Delta x/d = -0.027$. It is surmised that this could be caused by the up-wash (C'), essentially pushing $V_{1R'}$ upwards and $V_{2R'}$ in the +x-direction due to the skewness. Comparing the case of the rotating wheel at 5° yaw to the stationary results also presented in Figure 8, the application of yaw shows the two vortex wake on the stationary wheel propagating towards the windward side of the wheel, whilst the two vortex wake observed behind the rotating wheel is unable to fully entrain the two vortices towards the windward side. This was found to be as a result of the skewed up-wash & downwash on the stationary case entraining the flow more towards the windward side. However, due to the wheel rotation, the up-wash skewed at approximately θ=49° from the horizontal (Figure 8(a)-$\theta_{R'}$), interacts with the shear layer formed on top of the wheel which is also rotated towards the windward side, and causes the flow to circulate subsequently forming the vortical structures.

Article in International Journal of Computational Science and Engineering 14(4):370 · January 2017
DOI: 10.1504/IJCSE.2017.10005741

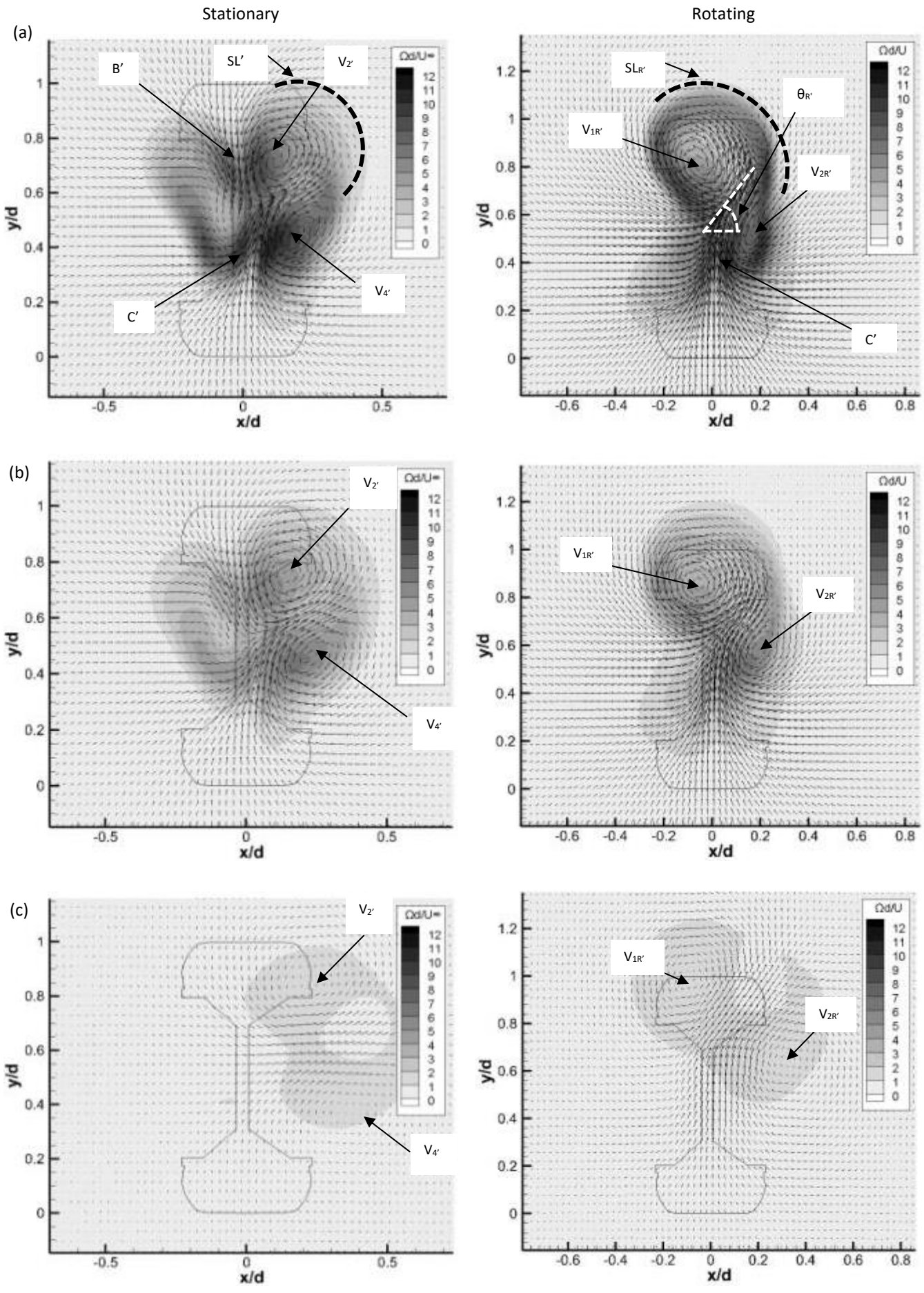

Figure 8. Non-dimensional vorticity plots for 53 yaw wheel; a) z/d=0.75, b) z/d=1, c) z/d=2.5 (Re_n =1.1 x10^6)

However, this slight increase in yaw angle remains unable to fully entrain the wake towards the windward side of the wheel. The two principal vortices were also found to be weaker in vorticity magnitude for the rotating case when compared to the stationary case by 64% & 77% for the upper ($V_{1R'}$) and lower ($V_{2R'}$) vortex respectively, at z/d = 0.75. This is also a trend which had been identified in previous studies comparing stationary and rotating wheels with zero applied wheel yaw [Mears et al. (2002)], as the vortices formed behind the stationary wheel are formed as the flow rolls over the shoulders of the wheel whilst being entrained by the up-wash and downwash from both the bottom and top of the wheel respectively. However, as the vortices behind the rotating wheel are formed upon interaction of the up-wash with the separated shear layer created further towards the top of the wheel, this results in a weaker vorticity magnitude for the rotating case when comparing both the stationary and rotating configurations at the same streamwise data plane at z/d=0.75.

With an incremental increase of another 5° to a 10° yaw angle, the wake dynamics illustrated in Figure 9 continue to show the dominant two vortex wake. However, with this additional increase in yaw angle, the two vortical structures have further translated more towards the windward side of the wheel (Figure 9-E.O.Y). The upper vortex ($V_{1R''}$) is now positioned at x/d = 0.066 and y/d = 0.824 whilst the lower vortex $V_{2R''}$ is positioned at x/d = 0.196 and y/d = 0.477 at z/d = 0.75, representing vortex core position displacements relative to the vortices on the 5° yaw case of $V_{1R''}$: $\Delta x/d = 0.121$, $\Delta y/d = 0.002$ and $V_{2R''}$: $\Delta x/d = 0.027$, $\Delta y/d = -0.041$. The subtle translation of $V_{1R''}$ in the vertical direction and the more noticeable transverse displacement together with both the transverse and vertical displacement of $V_{2R''}$ essentially shows the two vortical structures rotating clockwise towards the windward side (as seen from behind), suggesting that the influence of rotation is to enhance this skewness characteristic towards the windward side of the wheel with increasing yaw angle. At 5° yaw, the upper vortex ($V_{1R'}$) was positioned on the negative x/d side of the wheel (leeside) but with a further application of 5° yaw, both vortices are positioned on the positive x/d side (windward side), resulting most probably from the increased skewness in the up-wash (C'') displacing the wake towards the windward side whilst being entrained by the rotated shear layer ($SL_{R''}$ in Figure 9a).

Vortex core vorticity magnitude indicated $\Omega d/U_\infty = 5.60$ for $V_{1R''}$ and $\Omega d/U_\infty = 7.57$ for $V_{2R''}$ respectively, at z/d = 0.75; indicating a lower vortex stronger by up to 35%, which was somewhat expected due to the combination of the free-stream flow and wheel rotation travelling in the same direction, increasing the flow velocity entering the rear wake from the lower windward side of the wheel. Further downstream to z/d = 2.5, differences in central core vorticity magnitude reduce to $\Omega d/U_\infty = 1.59$ & $\Omega d/U_\infty = 1.73$ for $V_{1R''}$ and $V_{2R''}$ respectively.

With comparison of this 10° yaw rotating case to the stationary results also illustrated in Figure 9, it is clearly evident that the application of rotation has continued to form a taller wake which propagates in the vertical direction as y/d=1.02 for $V_{1R"}$ & y/d=0.82 for $V_{2"}$ & y/d=0.51 for $V_{2R'"}$ and y/d=0.297 for $V_{4"}$ at the furthest analysed downstream plane of z/d=2.5. This tends to indicate greater vertical vortex core position for the rotating case. This taller wake compared to the stationary case is also illustrated by the vertical distance of each vortex relative to x/d=0 & y/d=0 positions in Figure 9; Y_{1R} relative to Y_1 and Y_{2R} relative to Y_2 at z/d=0.75, with a similar trend at z/d=2.5. Additionally, the vertical displacement with downstream propagation from z/d=0.75 to z/d=2.5 is also illustrated in Figure 9 in a similar manner, $Y_{1R'}$ relative to Y_{1R} and $Y_{2R'}$ relative to Y_{2R}. However, the stationary wheel shows the wake being displaced further in the transverse direction towards the windward side indicated at z/d=2.5; x/d=0.17 for $V_{1R"}$ & x/d=0.36 for $V_{2"}$ & x/d=0.41 for $V_{2R"}$ and x/d=0.43 for $V_{4"}$. This result was likely due to the up-wash and downwash on the stationary wheel being skewed almost directly horizontal ($\theta"=10°$) to fully entrain the flow towards the windward side of the wheel, whilst the up-wash on the rotating wheel is skewed at a steeper angle ($\theta_{R"}\approx40°$) from the horizontal.

Article in International Journal of Computational Science and Engineering 14(4):370 · January 2017
DOI: 10.1504/IJCSE.2017.10005741

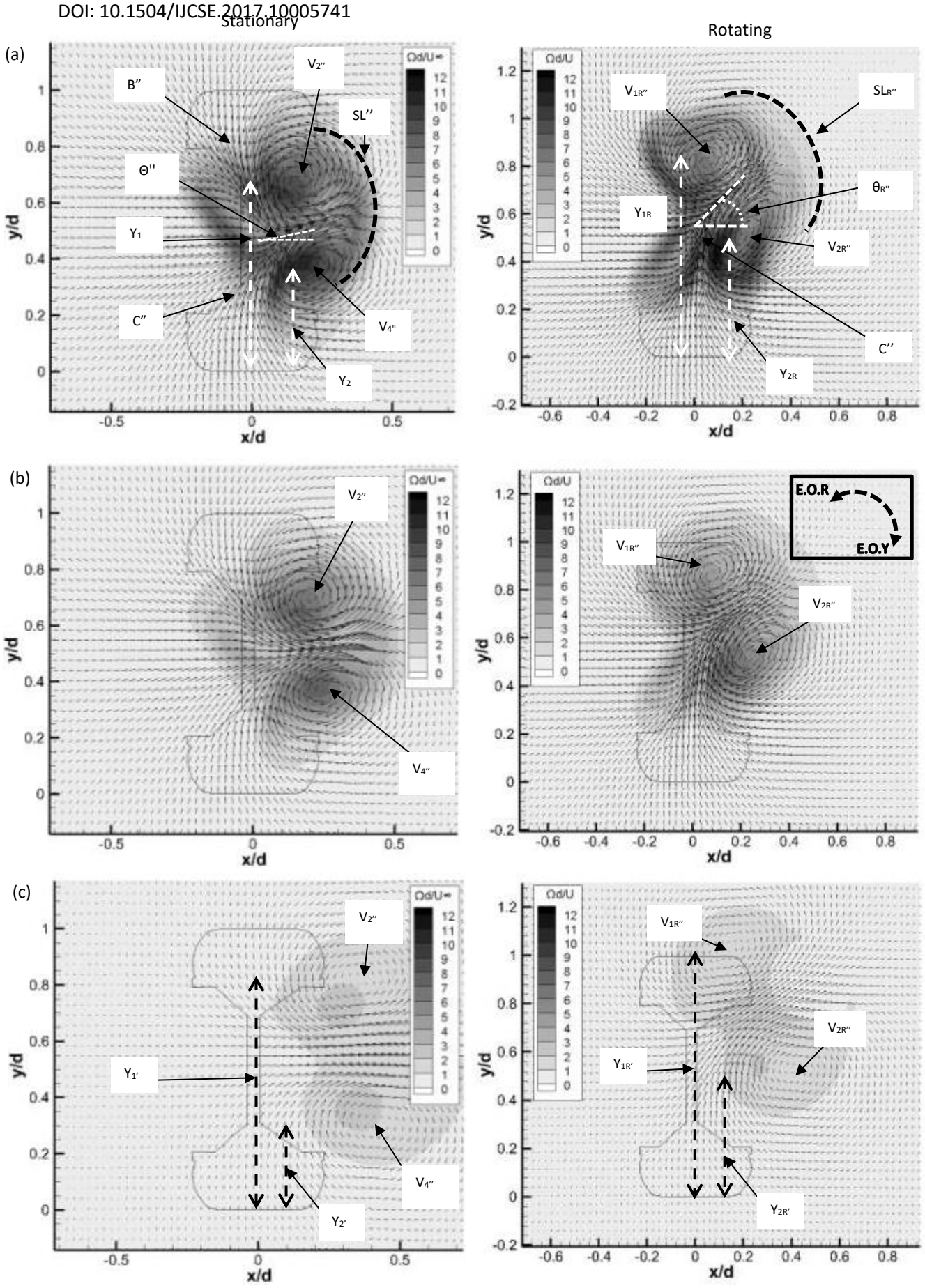

Figure 9. Non-dimensional vorticity plots for 10° yaw wheel; a) z/d=0.75, b) z/d=1, c) z/d=2.5
E.O.R = Effect of Rotation, E.O.Y = Effect of Yaw. (Re_n =1.1 x10^6)

With the maximum applied wheel yaw ($\Psi = 15°$) on the rotating wheel, the characteristics of the effect of rotation observed for the 5° and 10° cases were further intensified. Figure 10 illustrates the wake characteristics for this 15° yawed case, and its respective stationary results are also presented for comparison. The two dominant vortical structures are still present together with the up-wash (C'''), which is skewed further towards the windward side of the wheel at an angle of approximately $\theta_{R'''}=30°$ to the horizontal as shown in Figure 10. This skewness characteristic of the up-wash was found to enhance the clockwise translation of these two vortical structures towards the windward side of the wheel whilst being entrained by the rotated shear layer formed on the upper rear surface of the wheel. Additionally, the symmetry between the rear upper, and lower, halves of the wheel intensifies with increasing yaw angle, resulting in improved symmetry between the two vortices. Comparing the vortices formed in the rear wake of the 15° yaw case (Figure 10(a) - $V_{1R'''}$ and $V_{2R'''}$) relative to the vortices observed on the 10° yaw wheel (Figure 9(a) - $V_{1R''}$ and $V_{2R''}$) at z/d=0.5, the vortex core displacement for the upper vortex ($V_{1R'''}$) is $\Delta x/d = 0.12$, $\Delta y/d = -0.07$ and $\Delta x/d = -0.585$, $\Delta y/d = -0.09$ for the lower vortex $V_{2R'''}$. The increased skewness of the up-wash (C''') towards the windward side, reduces the vertical displacement of the two vortices, while increasing the transverse displacement. Considering both vortex core vorticity magnitudes at z/d = 0.75, $V_{1R'''}$ has a larger vortex core magnitude as $\Omega d/U_\infty = 8.10$ compared to $\Omega d/U_\infty = 7.41$ for $V_{2R'''}$. However, further downstream (z/d > 0.75) vorticity magnitude between the two vortices are almost identical, with a difference in vorticity magnitude of 3% between $V_{1R'''}$ & $V_{2R'''}$. Conversely, when compared to the stationary, 15° yawed wheel, the results obtained with applied rotation show a greater vertical position and displacement of the two vortices as is shown in Figure 10(c). This figure also illustrates the up-wash and downwash on the stationary case being skewed due to the applied yaw angle which also causes more horizontal movement towards the windward side of the wheel (A'''), and results in a near symmetric wake about the horizontal wheel centreline. However, for the rotating case, results illustrate this up-wash phenomenon rotated approximately 30° anticlockwise from the horizontal, resulting in the overall wake configuration also being skewed anticlockwise.

Overall, the results of the yawed rotating cases show that the vortical structures and overall wake are positioned closer towards the horizontal centreline of the wheel with increasing yaw angle (z/d=0.75 $\theta_R=49°$, $\theta_{R''}=40°$ and $\theta_{R'''}=30°$ approximately with 5°, 10° and 15° applied wheel yaw respectively - Figure 9 – E.O.Y). However, when comparing the rotating cases to their respective stationary case, the two primary vortical structures on the rotating case are observed to be rotated anticlockwise compared to the stationary results (Figure 9 – E.O.R). This was thought to occur as the resultant effect of the skewed up-wash behind the rotating wheel essentially displacing the wake in the vertical direction, as opposed to the up-wash and downwash behind the stationary wheel effectively entraining the wake towards the windward side of the wheel with increasing yaw angle. This is also illustrated by the rotated shear layer on the rotating case relative to its respective stationary case, (Figure 8a $SL_{R'}$ relative to SL', Figure 9a $SL_{R''}$ relative to SL'' and Figure 10a $SL_{R'''}$ relative to SL''') for each the 5°, 10° and 15° yawed configurations.

Article in International Journal of Computational Science and Engineering 14(4):370 · January 2017
DOI: 10.1504/IJCSE.2017.10005741

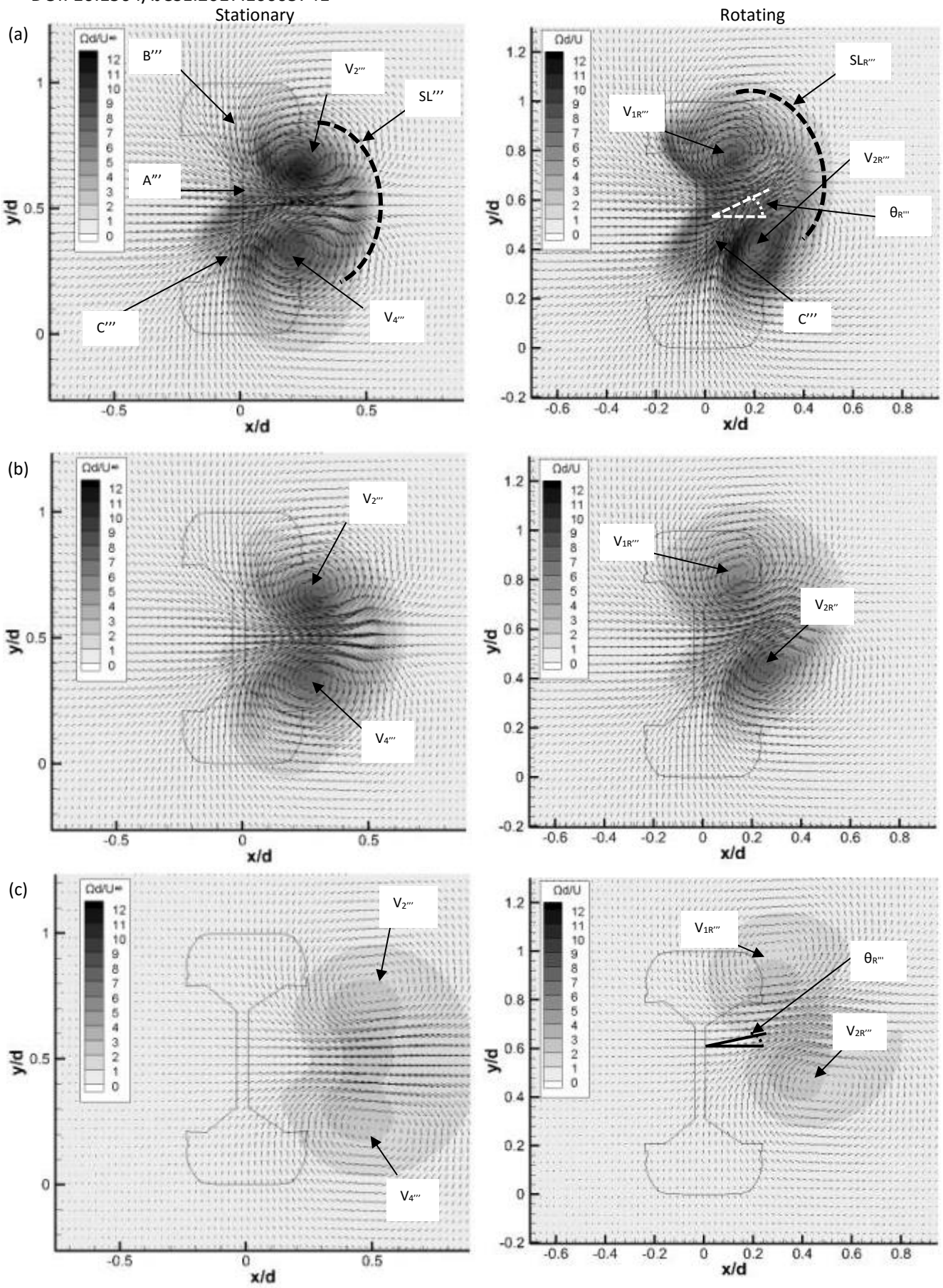

Figure 10. Non-dimensional vorticity plots for 15° yaw wheel; a) z/d=0.75, b) z/d=1, c) z/d=2.5 (Re_n =1.1 x10^6)

Article in International Journal of Computational Science and Engineering 14(4):370 · January 2017
DOI: 10.1504/IJCSE.2017.10005741

Vortex Core Positions

To further analyse the effect of applied yaw angle on a rotating wheel, the calculated relative displacement of the two dominant vortices (V_{1R}, V_{2R}) are illustrated in Figure 11 with downstream propagation referenced to the z/d = 0.75 plane($\Delta x/d = 0$, $\Delta y/d = 0$). Considering the lateral relative displacement ($\Delta x/d$), the results indicate an increasing lateral displacement towards the windward side of the wheel with increasing yaw angle. However, at Ψ=5°, the upper vortex ($V_{1R'}$) indicates a small displacement of $\Delta x/d = -0.03$ at the furthest downstream plane z/d = 2.5. This shift towards the leeside of the wheel was thought to be caused by the skewed up-wash not being able to fully entrain the flow towards the windward side of the wheel. At $\Psi \geq 10°$, the shear layer is rotated clockwise towards the upper windward side of the wheel causing regions of recirculation to be entrained within this region. Vortex core displacement on the non-yawed rotating wheel, Figure 7, shows V_{1R} propagating downstream on the leeside of the wheel (-x direction relative to the wheel centreline). Therefore with an additional increase in yaw angle to only 5°, the upper vortex V_{1R} continues to propagate on the leeside of the rotating wheel, with the transverse displacement for both vortices shown to have near-constant linear displacement downstream with increasing yaw angle. Considering the vortex core displacement in the vertical direction as shown in Figure 11(b), changes in vertical position are shown to be relatively small compared to the transverse direction with linear downstream vertical vortex core propagation also evident with increasing yaw angles. The one exception for this trend is the case of the lower vortex ($V_{2R'}$) on the 5° yaw configuration, however this non-linearity only occurs up until the z/d = 1 position downstream. Comparing the rotating cases in Figure 11 to the stationary results illustrated in Figure 14 [Kothalawala and Gatto (2015)], the most dominant difference with the application of yaw seems to be the direct transformation of the initially observed four vortex wake on an un-yawed stationary wheel to a two vortex wake, much more symmetrically positioned about the horizontal centreline of the wheel. Subsequently, with the application of rotation, the vertical displacement between the two vortices also becomes more symmetrical about the horizontal wheel centreline with increasing yaw angle, as shown in Figure 11(b). Additionally, application of the largest yaw angle on the rotating wheel (Ψ = 15°) showed increased symmetry between the two vortices about the horizontal centreline of the wheel ($\Delta y/d = 0.5$), however remaining skewed at an apparent up-wash angle. This has been shown in the past to be a common characteristic of the wake physics behind both a rotating cylinder and wheel in contact with the ground, as the effect of rotation displaces the wake at a net up-wash angle [Stapleford and Carr (1970), Seifert (2012)].

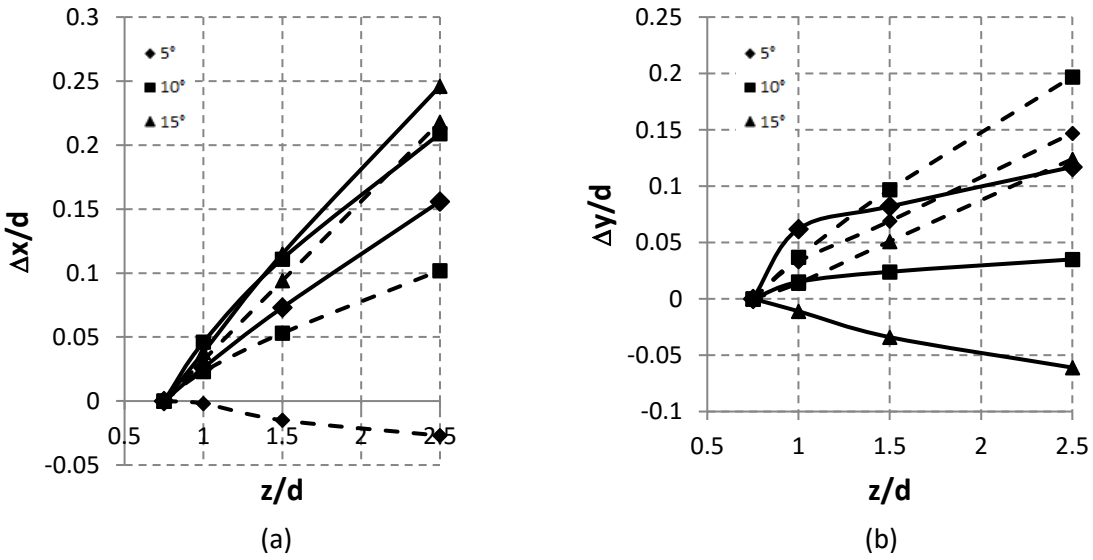

Figure 11. Vortex core displacements relative to z/d=0.75 with downstream propagation; V_{1R} (dashed), V_{2R} (solid) (Re_n =1.1 x10^6)

Article in International Journal of Computational Science and Engineering 14(4):370 · January 2017
DOI: 10.1504/IJCSE.2017.10005741

Overall Lift, Drag, and Side Force coefficients

From analysis of the rear wake physics on the rotating wheel with applied yaw angle, a larger wake region is created relative to the stationary case. This is a result of the application of yaw increasing the transverse displacement of the wake and vortices, together with the application of rotation increasing the vertical displacement of the rear wake. Table 1 shows the coefficients for drag, lift and side force for the rotating wheel with the assemble-averaged lift and drag coefficients for the baseline flow case on the rotating wheel with no applied yaw found to be C_L=-0.25 and C_D=0.44 respectively. The negative lift coefficient observed on this rotating case with zero applied wheel yaw was formed due to the pressure differential between the upper and lower surfaces (The Magnus Effect) [Zdravkovich (2003)]. From table 1, the drag force was observed to increase with the application of yaw, similar to the results obtained on the yawed wheel in contact with the ground by Sprot (2013). The larger rear wake region created by the larger spread of lateral velocity vectors [Axerio-Cilies et al (2012)] resulted in an overall 16% increase in drag force with increasing yaw angle to 15°. Whilst comparing the rotating and stationary configurations, it was observed that the difference between the drag coefficients reduced with increasing yaw angle; i.e. comparing the rotating cases relative to the stationary case 0° yaw: ΔC_D = 0.09, 5° yaw: ΔC_D = 0.08, 10° yaw: ΔC_D = 0.07, and 15° yaw: ΔC_D = 0.01. These results indicate that as the drag coefficient increases with increasing yaw angle on both cases, the C_D of the rotating case is still larger than the stationary cases as the wake is taller. Additionally the increased exposure of the windward side hub cavity with increasing yaw angle was found to increase the areas of hub stagnation, which would also contribute to the increased drag force. This increased exposure of the windward side hub cavity to the free-stream flow, at larger yaw angles, was also found to increase the side force magnitude acting towards the leeside of the wheel.

An observed increase in lift force coefficient was found to result from the combination of both yaw and rotation. While a negative lift force (acting downwards) is experienced on the non-yawed rotating wheel in agreement with the Magnus effect [Zdravkovich (2003)], with the application of yaw, the lift force coefficient was found to increase towards zero. This was observed to be due to the upper separation position being displaced from its initial position of θ=264° at 0° yaw to θ=247° at 15° yaw, (located further towards the back of the wheel), delaying flow separation and reducing the magnitude of the pressure differential between the upper and lower surfaces. This was found to be unique to the application of rotation as the application of only pure yaw showed no significant change to the lift force [Kothalawala and Gatto (2015)]. The results presented in Table 1 also show an increase in side force coefficient towards the leeside (negative x-direction), and would be expected as more of the windward side hub cavity is exposed to the oncoming flow with increasing yaw angle. This characteristic was found to be similar to the trend in side force experienced on the stationary cases, as detailed in Kothalawala and Gatto (2015).

Force Coefficient	**Wheel Yaw Angle**							
	0°		**5°**		**10°**		**15°**	
	Stationary	Rotating	Stationary	Rotating	Stationary	Rotating	Stationary	Rotating
Lift	-0.01	-0.25	-0.07	-0.24	-0.04	-0.21	0.02	-0.11
Drag	0.35	0.44	0.35	0.43	0.39	0.46	0.50	0.51
Side	-0.05	0.01	-0.18	-0.14	-0.35	-0.31	-0.52	-0.54

Table 1. Summary of lift, drag and side force coefficients for the yawed stationary & rotating wheel (Re_n =1.1 x10^6)

Article in International Journal of Computational Science and Engineering 14(4):370 · January 2017
DOI: 10.1504/IJCSE.2017.10005741

Conclusion

An Unsteady Reynolds-Averaged Navier-Stokes investigation has been carried out into the effects of yaw angle of the aerodynamics of a rotating isolated wheel in free-air. The fundamental findings into the effect of applied rotation on an isolated wheel were discussed in this paper and where possible, compared to previous work. Results from this investigation shows one of the key features of applied rotation is the reversed vortex formation characteristics with the direction of curl is reversed when compared to the stationary, isolated-wheel, cases. The application of rotation was also found to form a two vortex rear wake compared to the four vortex wake found behind a stationary wheel in free air. Due to the earlier separation positions on a rotating wheel, the rear wake was also displaced at an up wash angle with the application of yaw continuing to show a dominant two vortex wake. Additionally, with increasing yaw angle, the two vortex wake & the skewed up-wash was found to be rotated clockwise towards the windward side (when looking from behind) with increased symmetry between the vortical structures enclosed within the upper and lower halves of the rear wake. Overall, the application of increasing yaw angle on the rotating wheel highlighted a clockwise translation of the two vortex rear wake, as the angle of the skewed up-wash decreased by approximately 10° with every 5° incremental increase in yaw angle. Force coefficients were also presented, with the identifiable trend being an increase in the lift force coefficient, with increase yaw angle.

References

Ansys Fluent Theory Guide, Release 13.0. (2010)

Axerio-Cilies, J., Issakhanian, E., Jimenez, J. and Iaccarino, G. (2012) 'An aerodynamic investigation of an isolated stationary formula 1 wheel assembly', *ASME Journal of Fluids Engineering*, Vol. 134, No. 2, pp.121101-1–121101-16.

Axon, L. (1998) *The Aerodynamic Characteristics of Automobile Wheels – CFD Prediction and Wind Tunnel Experiment*, PhD dissertation, College of Aeronautics, Cranfield University.

Bayraktar, E., Mierka, O. and Turek, S. (2012) 'Benchmark computations of 3D laminar flow around a cylinder with CFX, OpenFOAM and FeatFlow', *Int. J. Computational Science and Engineering*, Vol. 7, No. 3, pp.253–266.

Benim, A.C., Nahavandi, A. and Syed, K.J. (2005) 'URANS and LES analysis of turbulent swirling flows', *Progress in Computational Fluid Dynamics*, Vol. 5, No. 8, pp.444–454.

Benim, A.C., Pasqualotto, E. and Suh, S.H. (2008) 'Modelling turbulent flow past a circular cylinder by RANS, URANS, LES and DES', *Progress in Computational Fluid Dynamics*, Vol. 8, No. 5, pp.299–307.

Bursnall, W. and Loftin, L. (1951) *Experimental Investigation of the Pressure Distribution about a Yawed Circular Cylinder in the Critical Reynolds Number Range*, National Advisory Committee for Aeronautics Technical Note 2463.

Cogotti, A. (1983) 'Aerodynamic characteristics of car wheels', *International Journal of Vehicle Design, Special Publication SP3*, pp.173–196.

Dimitriou, I. and Klussmann, S. (2006) 'Aerodynamic forces of exposed and enclosed rotating wheels as an example of the synergy in the development of racing and passenger cars', *2006 SAE World Congress and Exhibition*, 2006-01-0805.

Dobrzynski, W. (2010) 'Almost 40 years of airframe noise research: What did we achieve?', *Journal of Aircraft*, Vol. 47, No. 2, pp.353–367.

Fackrell, J.E. (1974) *The Aerodynamics of an Isolated Wheel Rotating in Contact with the Ground*, PhD thesis, University of London, UK.

Fackrell, J.E. and Harvey, J.K. (1975) 'The aerodynamics of an isolated road wheel', *AIAA Proceedings of the Second Symposium on Aerodynamics of Sports and Competition Automobiles*, North Hollywood, CA.

Gerrard, J. (1966) 'The three-dimensional structure of the wake of a circular cylinder', *Journal of Fluid Mechanics*, Vol. 25, No. 1, pp.143–164.

Hedges, L.S., Travin, A.K. and Spalart, P.R. (2002) 'Detached-eddy simulations over a simplified landing gear', *Journal of Fluids Engineering*, Vol. 124, No. 2, pp.413–423.

Jones, K. (2009) *Aircraft Noise and Sleep Disturbance: A Review*, Environmental Research and Consultancy Department, ERCD 0905.

Kaennakham, S. and Moatamedi, M. (2014) 'An automatic mesh adaptation algorithm and its performance for simulation of flow over a circular cylinder at Re = 1.4 × 105', *Int. J. Computational Science and Engineering*, Vol. 9, No. 3, pp.257–273.

Knottnerus, J.A. (2004) *The Influence of Night-time Noise on Sleep and Health*, Health Council of the Netherlands, publication no. 2004/14E.

Kothalawala, T.D., and Gatto, A. (2015) 'Computational Investigation into the Influence of Yaw on the Aerodynamics of an Isolated Wheel in Free Air', International Journal of Computational Science and Engineering. (In-Press)

Lan, Z., and Deshikachar, P. (2004) 'Performance analysis of a large-scale cosmology application on three cluster systems', Int. J. High Performance Computing and Networking, Vol. 2, Nos. 2/3/4, pp. 156-164

Lazos, B.S. (2002a) 'Mean flow features around the inline wheels of four-wheel landing gear', *Journal of Aircraft*, Vol. 40, No. 2, pp.193–198.

Lazos, B.S. (2002b) 'Surface topology on the wheels of a generic four-wheel landing gear', *J. Aircraft*, Vol. 40, No. 2, pp.2402–2411.

Li, F., Khorrami, M. R., and Malik, M. R., (2002) "Unsteady Simulation of a Landing-Gear Flowfield," *AIAA*, pp. 1-12.

Logg, A. (2009) 'Efficient representation of computational meshes', *Int. J. Computational Science and Engineering*, Vol. 4, No. 4, pp.283–295.

Luo, L-S., Krafczyk, M., and Shyy, W. (2010) 'Lattice Boltzmann Method for Computational Fluid Dynamics', Encyclopaedia of Aerospace Engineering, Chapter 56, pp. 651-660.

MacCarthy, N.H. (2010) *An Experimental Study of the Aerodynamics of Exposed Wheels*, PhD, Department of Aeronautics, Imperial College.

McManus, J. and Zhang, X. (2006) 'A computational study of the flow around an isolated wheel in contact with ground', *Journal of Fluids Engineering*, Vol. 128, No. 3, pp.520–530.

Mears, A. P., Dominy, R.G., and Sims-Williams, D.B., 'The Air Flow about an Exposed Racing Wheel', *SAE International*, 2002.

Mears, A.P. (2004) *The Aerodynamic Characteristics of an Exposed Racing Car Wheel*, PhD thesis, University of Durham.

Mercker, E. and Berneburg, H. (1992) 'On the simulation of road driving of a passenger car in a wind tunnel using a moving belt and rotating wheels', *3rd International Conference of Innovation and Reliability*, Florence, 8–10 April.

Article in International Journal of Computational Science and Engineering 14(4):370 · January 2017
DOI: 10.1504/IJCSE.2017.10005741

Seifert, J. (2012) 'A review of the Magnus effect in aeronautics', *Progress in Aerospace Sciences*.

Smith, R.A., Moon, W.T., and Kao, T.W. (1972) "Experiments on Flow about a Yawed Circular Cylinder," *Journal of Basic Engineering*, pp. 771-776.

Sprot, A. J., (2013) 'Open-Wheel Aerodynamics: Effects of Tyre Deformation and Internal Flow'. Durham theses. Durham University.

Stapleford, W.R. and Carr, G.W. (1970) *Aerodynamic Characteristics of Exposed Rotating Wheels*, Technical Report 1970/2, Motor Industry Research Association.

Wray, J. (2003) *A CFD Analysis Into the Effect of Yaw Angle on the Flow Around an Isolated Rotating Wheel*, MSc, Cranfield College of Aeronautics, Cranfield University.

Zdravkovich, M.M. (2003) *Flow Around Circular Cylinders*, Oxford University Press

Zdravkovich, M.M., Brand, V.P., Mathew, G. and Weston, A. (1989) 'Flow past short circular cylinders with two free ends', *Journal of Fluid Mechanics*, Vol. 203, pp.557–575.

Zhang, X., Ma, Z., Smith, M. and Sanderson, M. (2013) 'Aerodynamic and acoustic measurements of a single landing gear wheel', *AIAA, 19th AIAA/CEAS Aeroacoustics Conference*.